Available online at www.sciencedirect.com

SciVerse ScienceDirect

Ceramics International 39 (2013) 4407–4412

CERAMICS INTERNATIONAL

www.elsevier.com/locate/ceramint

Effect of sintering temperature on the electric properties and microstructure of SnO_2–Co_3O_4–Sb_2O_5–Cr_2O_3 varistor ceramic

J.A. Aguilar-Martínez[a,*], M.I. Pech Canul[b], M.B. Hernández[c], A.B. Glot[d], Edén Rodríguez[c], L. García Ortiz[c]

[a]*Centro de Investigación en Materiales Avanzados, S.C. (CIMAV), Parque de Investigación e Innovación Tecnológica (PIIT), Alianza Norte No. 202, Nueva carr. Aeropuerto km. 10, C.P. 66600 Apodaca N.L., México*

[b]*Centro de Investigación y de Estudios Avanzados del Instituto Politécnico Nacional, Unidad Saltillo. Av. Industria Metalúrgica No. 1062, Parque Industrial, Ramos Arizpe Coah., C.P. 25900, México*

[c]*Facultad de Ingeniería Mecánica y Eléctrica, Universidad Autónoma de Nuevo León, San, Nicolás de los Garza, N.L. México*

[d]*Departamento de Posgrado; Universidad Tecnológica de la Mixteca, Carr. Acatlima Km. 2.5, Huajuapan de León Oaxaca C.P. 69000, México.*

Received 12 October 2012; received in revised form 7 November 2012; accepted 13 November 2012
Available online 21 November 2012

Abstract

SnO_2 varistors doped with Co_3O_4, Cr_2O_3, and Sb_2O_5 were prepared by a high-energy milling planetary method. The sintering temperature of the varistors was optimized to improve the electrical properties, nonlinearity coefficient and breakdown electric field. The best results were achieved at a sintering temperature of 1350 °C, obtaining a nonlinear coefficient of 33 and a breakdown electric field of 2620 V cm^{-1}. The samples obtained at all sintering temperatures showed not only high density values, reaching 90.5% of the theoretical density, but also the resulting microstructure was optimized in such a way that the varistors compete with those obtained by chemical methods, with the advantage that the milling planetary method is cheaper, faster and easier than chemical routes. Based on substitution equations using the Kröger–Vink standard notation, an attempt is made elucidate the role of each of the dopants. A processing-microstructure-property correlation is also reasonably established.

Keywords: A. Sintering; B. Grain size; C. Electrical properties; D. High-energy milling

1. Introduction

Varistors are ceramic semiconductor devices with highly nonlinear current–voltage characteristics. These materials are commonly used as over-voltage and surge absorbers in electronic circuits and electrical systems [1–4]. The current–voltage ($j(E)$) characteristic of varistor ceramics is frequently approximated by the empirical power-law relation

$$j = kE^{\alpha}, \tag{1}$$

where j is the current density, E is the average electric field, k and α are constants. The degree of the nonlinearity of current–voltage characteristic is estimated by the nonlinearity coefficient [5]:

$$\alpha = \frac{\rho_s}{\rho_d} = \frac{E}{j}\frac{dj}{dE} = \frac{d(\mathrm{In}j)}{d(\mathrm{In}E)} \tag{2}$$

giving the ratio of the static resistivity $\rho_s = E/j$ to the differential resistivity $\rho_d = dE/dj$at fixed current density, where nonlinearity is high. The integration of Eq. (2) at a condition $\alpha =$ constant gives the expression (1). The nonlinearity coefficient α and the electric field strength E are considered as the main parameters of varistor ceramics. The greater the value of α, the better the device.

Since it was introduced by Matsuoka, back in 1971, zinc oxide (ZnO) has been the most extensively studied material (as the base for a ceramic system) and consequently became the most important ceramic for the commercial production of varistors [3,6]. Due to the need for better

*Corresponding author. Tel.: +52 81 11560805; fax: +52 81 11560820.
E-mail addresses: josue.aguilar@cimav.edu.mx, jaguilar_mtz@hotmail.com (J.A. Aguilar-Martínez).

0272-8842/$ - see front matter © 2012 Elsevier Ltd and Techna Group S.r.l. All rights reserved.
http://dx.doi.org/10.1016/j.ceramint.2012.11.030

properties, recently there has been increased interest in other ceramic materials like TiO_2 [7], $SrTiO_3$ [8], WO_3 [9], CeO_2 [10] and SnO_2 [11].

Tin dioxide (SnO_2) is an *n*-type semiconductor with the rutile-type structure and space group D_{4h}^{14} $[P4_2/mnm]$ [12]. Tin dioxide exhibits interesting physical properties suitable for various applications [12–15]. Recently there has been a growing interest in the development of SnO_2-based varistor [11,16]. Some fact that restricts the application of this oxide is its low densification rate during sintering because of the predominance of non-densifying mechanisms for mass transport, such as surface diffusion (at low temperatures) and evaporation-condensation (at high temperatures) which only promote pure coarsening and grain growth [17]. This mechanism is triggered by the easy evaporation of SnO_2 at high temperatures. This can depicted by

$$SnO_2(s) \rightarrow SnO + \frac{1}{2}O_2\uparrow \tag{3}$$

However, tin dioxide dense ceramics can be obtained by the introduction of densifying agents, such as CuO, ZnO, CoO, and MnO_2 [17–20] or hot isostatic pressure processing [21], which promotes the densification of SnO_2 almost to the theoretical density value. The processing of SnO_2-based material with high density allows considering the ceramic as a promising material in electronic devices such as varistors.

In our work, (Co,Cr Sb)-doped SnO_2 ceramics were prepared, and the effect of sintering temperature on the physical and electrical properties of the SnO_2–Co_3O_4–Cr_2O_3–Sb_2O_5 varistors was investigated.

2. Experimental procedure

The raw chemicals used in this work, SnO_2 (Baker), Co_3O_4 (Baker), Sb_2O_5 (Aldrich) and Cr_2O_3 (Baker) were of analytical grades. The molar composition of the investigated systems was 95.49%SnO_2–4.38%Co_3O_4–0.05%Sb_2O_5–0.08%Cr_2O_3. The powders were processed by a non conventional method of mixture, through high-energy milling performed in a planetary ball-mill Pulverisette P7/2 (Fristsh GmbH, Germany) using vials and balls of agate for 20 min. The resulting powders were uniaxially pressed in the form of tablets (10.0 mm in diameter and about 1.2 mm thick) at 230 MPa without using any kind of binder. The tablets were sintered in ambient atmosphere at 1350, 1375, 1400, 1425 and 1450 °C for 1 h with a heating and cooling rate of 6 °C/min in a tube furnace (Lindberg/Blue STF55433C-1). For electrical characterization, silver electrodes were place on both faces of the ceramic sintered samples followed by thermal treatment at 800 °C for 6 min. Current–voltage measurements were taken using a high voltage measure unit (Keithley 237). The nonlinear coefficient α was evaluated in terms of the relation:

$$\alpha = \frac{\log(J_2/J_1)}{\log(E_2/E_1)}, \tag{4}$$

where E_1 and E_2 are the applied electric field corresponding to the current densities J_1 and J_2 respectively. The breakdown voltage (E_b) was obtained at 1 mA/cm^2. The J and E can be obtained through I/s and V/t, where s is the area of silver electrode and t *is* the thickness of the tested sample. The grain voltage (V_b) was estimated as:

$$V_b = \frac{E_b}{n}, \tag{5}$$

where, E_b is the breakdown electrical field, and n is the number of grains per unit length calculated from:

$$n = \frac{L}{G}, \tag{6}$$

being L the sample thickness and G the mean grain size.

The values of linear shrinkage γ were calculated according to the expression:

$$\gamma = \frac{D_0 - D}{D_0} \tag{7}$$

where D_0 and D are diameters of the sample before and after sintering, respectively.

Density measurements of the sintered samples were made using the Archimedes method and the percentage of residual porosity was calculated using the following formula:

$$\%P = \left(1 - \frac{\rho_{\text{Samples}}}{\rho_{\text{Theoretical}}}\right) \times 100, \tag{8}$$

where ρ_{sample} is the measured density of the sample and $\rho_{\text{Theoretical}}$ is the theoretical density of the sample calculated using the rule of mixtures:

$$\rho_c = \sum f_i \rho_i = f_1\rho_1 + f_2\rho_2 + \cdots + f_n\rho_n \tag{9}$$

where ρ_c is density of the simple, ρ_1, ρ_2, …, ρ_n are the densities of each component within the simple and f_1, f_2, …, f_n are the volume fractions of each component.

Scanning electron microscopy (SEM) (Philips XL30 ESEM) allowed the microstructural analysis of the sintered samples. The mean grain size was determined by analyzing SEM micrographs using the Image Analysis Software (Image-Pro Plus 4), ASTM-E112 standard procedures. Grain and grain boundary compositions were investigated by energy dispersive X-rays (EDX, EDAX). The ball-milled powders and all sintered samples were characterized by X-ray diffraction (XRD) using Cu Kα radiation in a Philips diffractometer, for which the X-ray diffraction patterns were collected at room temperature for 2θ degrees between 15 and 80° in steps of 0.02°.

3. Results and discussion

Fig. 1 shows the XRD patterns of the reference material (without sintering) and specimens sintered at 1350, 1375,

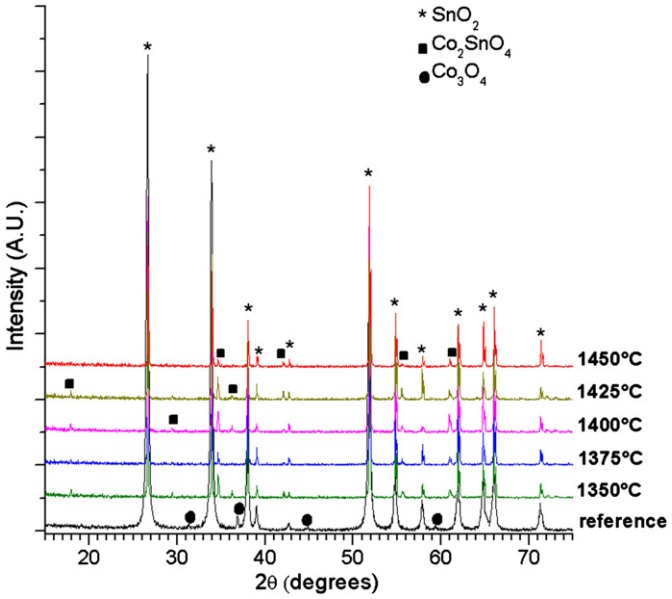

Fig. 1. X-ray diffraction patterns for the powder utilized (reference) and sintered samples at 1350, 1375, 1400, 1425 and 1450 °C.

Table 1
Densities, shrinkage and residual porosity of the sintered samples.

Sintering temperature (°C)	Shrinkage γ, (%)	Density ρ (g/cm^3)	Relative density ρ_r (%)	Residual porosity (%)
1350	19	6.216 ± 0.052	90.48	9.51
1375	19	6.200 ± 0.026	90.25	9.74
1400	19	6.252 ± 0.015	91.00	8.99
1425	19	6.110 ± 0.009	88.94	11.05
1450	19	6.245 ± 0.008	90.90	9.09

Theoretical density of samples sintered: 6.87 g/cm^3 obtained from the rule of mixtures.

1400, 1425 and 1450 °C. It is worth noting that SnO_2 peaks appear in all the diffractograms, while Co_3O_4 is detected only in the reference material. On the other hand, the Co_2SnO_4 phase is identified in all sintered specimens. The absence of Co_3O_4 and the presence of Co_2SnO_4 in the sintered specimens are closely related and explained in terms of the decomposition reaction undergone by Co_3O_4 as will be shown in the next paragraphs. The use of 4.38 mol% Co_3O_4 in this work confirms a statement reported in previous work [19] in which it is mentioned that in the tin oxide varistor system, the Co_2SnO_4 phase is formed when cobalt oxide is used in amounts exceeding 2 mol%.

The relative theoretical density (ρ_{rt}) of all samples was determined by the Archimedes method and the theoretical density was obtained by the rule of mixture as shown in Table 1, considering $\rho_{SnO_2} = 6.95$ g/cm^3, $\rho_{Co_3O_4} = 6.07$ g/cm^3, $\rho_{Sb_2O_5} = 3.78$ g/cm^3 and $\rho_{Cr_2O_3} = 5.22$ g/cm^3. It can be seen that the density of all samples is around 90% of the theoretical density. The porosity was calculated by Eq. (6) for all samples sintered and resulting values are between 9 and 11%. It should be noted that irrespective of the sintering temperature, all specimens experienced a similar shrinkage of 19% ascribed to the sintering phenomena. The residual porosity is made evident in the microstructure, associated to the formation of the spinel phase as agglomerates, as shown in the SEM photomicrographs of Fig. 2. This is more notorious in Fig. 2a and b, where the white phase corresponds to SnO_2, the gray phase to Co_2SnO_4 and the small dark regions, to porosity. The photomicrographs in Fig. 2a–e also show an apparent increment in grain size with increasing sintering temperature.

Fig. 3 shows representative logarithmic graphs of current density as a function of voltage for specimens sintered at 1350, 1375, 1400, 1425 and 1450 °C, from which the nonlinear coefficient (α) and breakdown electric voltage E_b were calculated. The magnitudes of α and E_b, together with the grain size and the grain voltage V_b (last column) are summarized in Table 2. Since the breakdown electrical field tends to decrease and the grain size to increase with sintering temperature and as the thickness of the specimen is constant, then, the grain voltage will also tend to decrease. Accordingly, and based also on the microstructure characteristics (percentage porosity, grain size, shown in Tables 1 and 2), the optimum temperature to enhance the nonlinear coefficient is 1350 °C.

In the following paragraphs an attempt is made to explain the role of each of the dopants and the phenomena occurring with SnO_2, together with a correlation of the processing with the microstructure and properties. The role of the dopants is explained with the aid of substitution equations, using the Kröger–Vink standard notation. This notation has been used to represent point defects in the SnO_2 lattice at the high-firing temperature. In general terms, these defects are represented by a main symbol followed by a superscript and a subscript. The main symbol is either the species involved, i.e., chemical symbol of an element, or the letter V for a vacancy; electronic defects also may be found as free electrons (which are in the conduction band of the crystal) designated as e. The subscript is either the crystallographic position occupied by the species involved or the letter i for interstitial atoms. The superscript denotes the effective electric charge on the defect, defined as the difference between the real charge of the defect species and that of the species that would have occupied that site in a perfect crystal. The superscript is a prime ($'$) for each negative charge, a dot ($\bullet$) for every positive charge, or an (x) for zero effective charge.

It is generally accepted that at high temperatures, tin oxide does not densify during sintering due to the high vapor pressure of this oxide, as represented by means of Eq. (3). Moreover, oxygen vacancies and tin interstitials would be produced in the SnO_2 lattice at a high-firing temperature, a process represented by the following two equations:

$$SnO_2 \rightarrow Sn''_{Sn} + V_O^{\bullet\bullet} + O_O^X + \tfrac{1}{2}O_2 \quad (10)$$

$$SnO_2 \rightarrow V''''_{Sn} + Sn_i^{\bullet\bullet\bullet\bullet} + 2O_O^X \quad (11)$$

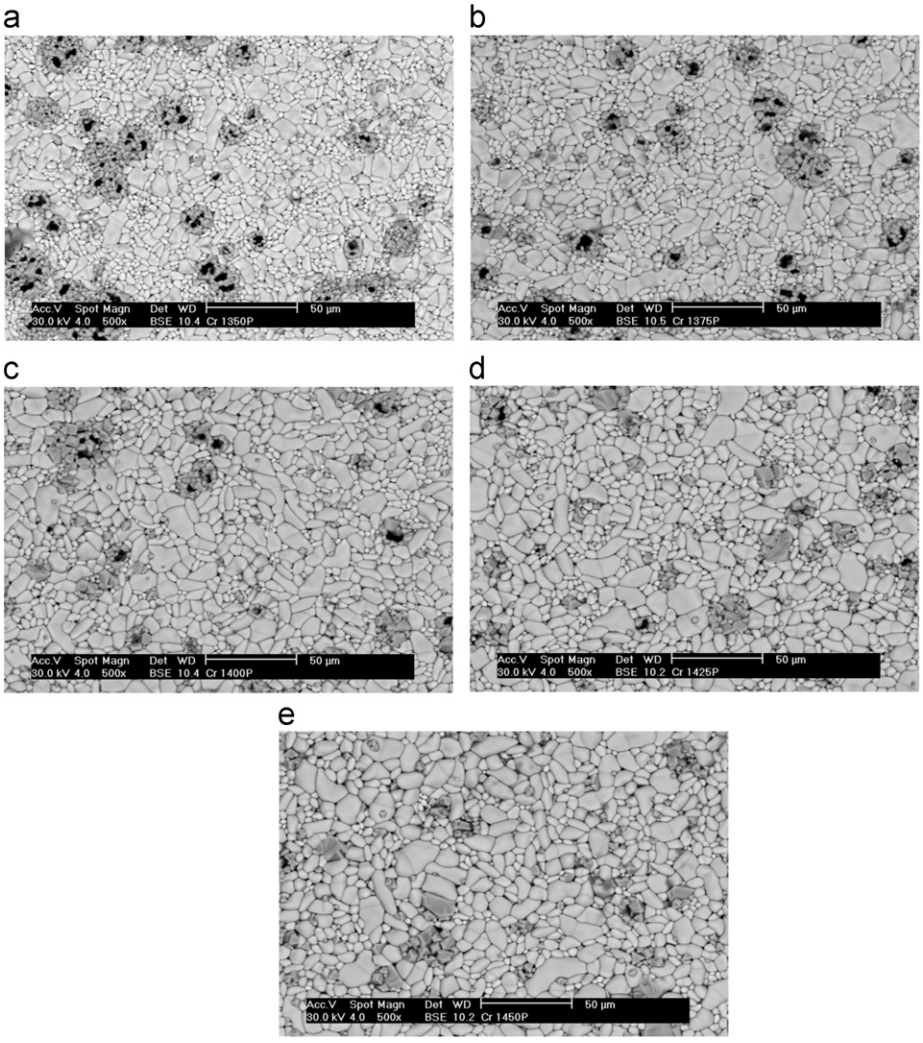

Fig. 2. SEM photomicrographs of sintered samples at a)1350, b)1375, c)1400, d)1425 and e)1450 °C.

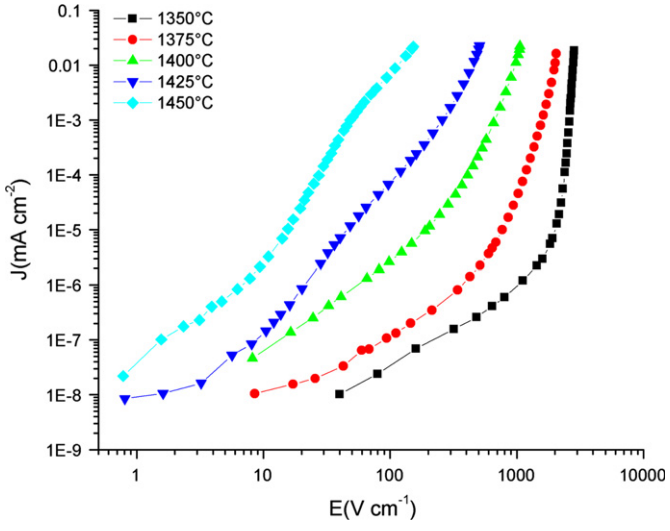

Fig. 3. *J–E* logarithmic plots for all samples.

The high densities obtained in the studied samples can be attributed to the addition of 4.38 mol% Co_3O_4 to the studied ceramic system. This oxide induces modifications in the oxygen vacancy concentration and promotes densification [22]. At high temperatures, Co_3O_4 may decompose in two possible ways, one of them having oxygen and CoO as reaction products, and the other, leading to CoO and Co_2O_3 as products. The first one is represented as follows [23]:

$$2Co_3O_4 \xrightarrow{850^{\circ}C} 6CoO + O_2 \quad (12)$$

Consequently, cobalt exhibits Co^{2+} oxidation state. The substitution of Sn^{4+} ions by Co^{2+} leads to the formation

Table 2
Effect of the sintering temperature on the electrical properties, average grain size and grain voltage.

Sintering temperature (°C)	α	E_b (V/cm)	Grain size (μm)	V_b (V/b)
1350	33	2620	4.49	1.17
1375	10.3	1620	4.88	0.79
1400	6.3	656	6.30	0.41
1425	4.3	258	6.91	0.17
1450	2.7	48	7.34	0.03

of oxygen vacancies and can presumably account for the densification of tin dioxide. These changes can be explained with the aid of replacement equations representing phenomena occurring in the tin oxide lattice. Possible substitution equations related to the role of CoO resulting from Co_3O_4 dissociation are as follows:

$$CoO \xrightarrow{SnO_2} Co''_{Sn} + V_O^{\bullet\bullet} + O_O^x \quad (13)$$

$$CoO \xrightarrow{SnO_2} Co''_{Sn} + 2V_O^{\bullet} + \tfrac{1}{2}O_2\uparrow \quad (14)$$

The second decomposition reaction for Co_3O_4 is given by the following equation:

$$Co_3O_4 \rightarrow CoO + Co_2O_3 \quad (15)$$

Likewise, possible substitution equations entailing the formation of oxygen vacancies are:

$$Co_2O_3 \rightarrow 2Co'_{Sn} + V_O^{\bullet\bullet} + 3O_O^x \quad (16)$$

$$Co_2O_3 \rightarrow 2Co'_{Sn} + 2V_O^{\bullet} + 2O_O^x + O_2 \quad (17)$$

$$V_O^{\bullet\bullet} + e' \rightarrow V_O^{\bullet} \quad (18)$$

The likelihood of the occurrence of these reactions is supported by previous works in which CoO is used as sintering agent [24]. C.-B. Wang and co-workers used CoO in their work and argued that at temperatures above 500 °C, CoO is oxidized by air to Co_3O_4, but that around 1000 °C, Co_3O_4 is subsequently decomposed back to CoO. In this context, if the role of cobalt oxide is to promote oxygen vacancy generation for densification, thus it is suggested that it is better to use Co_3O_4 instead of CoO, as in the present work, because it is the cobalt reduction reaction the one that entails oxygen vacancy formation. CoO formation by the dissociation of Co_3O_4 also helps in explaining the appearance of the spinel phase in the microstructure of sintered specimens, as shown in the characterization by XRD (Fig. 1). The Co_2SnO_4 spinel phase is formed according to the following reaction:

$$2CoO + SnO_2 \rightarrow Co_2SnO_4 \quad (19)$$

A detailed description of Co_2SnO_4 formation, based in a pathway determined using simultaneous thermal analysis (TGA/DSC) is presented elsewhere by the same research group [25].

As for the role of antimony oxide, without this dopant the sample appears as an insulator, because of the ultra-high grain resistivity. However, the introduction of Sb^{+5} ions in small amounts into the SnO_2 ceramics leads to the concentration of e' and V''''_{Sn}, which increases the electronic conductivity in the SnO_2 lattice and leads to the semi-conductivity of the grains. In terms of the Kröger–Vink notation this can be represented through the following possible reactions:

$$Sb_2O_5 \xrightarrow{SnO_2} 2Sb_{Sn}^{\bullet} + 2e' + 4O_O^x + \tfrac{1}{2}O_2\uparrow \quad (20)$$

$$Sb_2O_5 \xrightarrow{SnO_2} 4Sb_{Sn}^{\bullet} + V''''_{Sn} + 10O_O^X \quad (21)$$

Sb_2O_5 can also dissociate according to:

$$Sb_2O_5 \Leftrightarrow Sb_2O_3 + O_2 \quad (22)$$

and therefore, the following substitution reaction can also occur, with oxygen vacancy formation:

$$Sb_2O_3 \xrightarrow{SnO_2} 2Sb'_{Sn} + V_O^{\bullet\bullet} + 3O_O^X \quad (23)$$

The effect of Cr_2O_3 has been extensively investigated, originally on multicomponent ZnO varistors [26]. In ZnO ceramics it was found that improves the electrical properties of the varistors, but the increase in concentration has a deleterious effect on the potential barrier at the grain boundary. In SnO_2 varistors it is suggested that Cr_2O_3 inhibits tin oxide grain growth and densification of the samples [27]. In addition it results in the formation of two types of grains, differing in size and morphology. It was also reported that Cr_2O_3 facilitates the homogeneous enrichment of grain boundaries with oxygen species, increasing the performance of the nonohmic features of SnO_2-based varistor system [28]. The addition of Cr_2O_3 to the SnO_2 lattice leads to the substitution of Sn^{+4} by Cr^{+3} ions, according to the following reaction:

$$Cr_2O_3 \xrightarrow{SnO_2} 2Cr'_{Sn} + V''_O + 2O_O^x + \tfrac{1}{2}O_2\uparrow \quad (24)$$

It is important to recognize that the phenomena occurring at lattice level affects the overall microstructure, starting with the varistor's composition, reflected in the detected phases. It also influences the current–voltage response and the physical properties (density, residual porosity, etc.). In this regard, the fact that the relative theoretical density does not improve with increase in the sintering temperature and that the shrinkage is the same, leads to the conclusion that it is not necessary to using sintering temperatures above 1350 °C. This condition results in a desirable high value for α and also in a high value for E_b, suggesting that the varistor is suitable for high voltage applications. Therefore it is fair to say that the best results were achieved at the sintering temperature of 1350 °C, obtaining a nonlinear coefficient of 33 and a breakdown electrical field of 2620 V cm^{-1}.

4. Conclusions

In this work, the effect of sintering temperature on the microstructure, physical and electrical properties of SnO_2 varistors doped with Co_3O_4, Cr_2O_3, and Sb_2O_5 was investigated. The results show that sintering at the lowest temperature of 1350 °C is sufficient to obtain the highest nonlinear coefficient, though also with a high value of breakdown voltage that makes the varistor suitable for high voltage applications. Sintering at higher temperatures results impractical because: i) lowers the magnitude of α, ii) does not increase the density of the specimens and, iii) promotes grain growth. Based on substitution reactions by the Kröger–Vink standard notation, an attempt has been

made to explain the role of each of the dopants and their influence on the microstructure and electrical properties.

Acknowledgments

Authors gratefully acknowledge Mr. Miguel Esneider for his valuable help in determining grain size of studied samples.

References

[1] L. Levinson, H. Philipp, ZnO varistors for transient protection, IEEE Transactions Parts, Hybrids, and Packaging 13 (1977) 338–343.
[2] T.K. Gupta, Application of zinc oxide varistors, Journal of the American Ceramic Society 73 (1990) 1817–1840.
[3] D.R. Clarke, Varistor ceramics, Journal of the American Ceramic Society 82 (1999) 485–502.
[4] M. Peiteado, Varistores cerámicos basados en óxido de cinc, Boletín de la Sociedad Española de Ceramica 44 (2005) 77–87.
[5] A.B. Glot, A model of non-ohmic conduction in ZnO varistors, Journal of Materials Science: Materials in Electronics 17 (2006) 755–765.
[6] M. Matsuoka, Nonohmic properties of zinc oxide ceramics, Japanese Journal of Applied Physics 10 (1971) 736–746.
[7] S. Luo, Z. Tang, J. Li, Z. Zhang, Effect of Ta_2O_5 in (Ca, Si, Ta)-doped TiO_2 ceramic varistors, Ceramics International 34 (2008) 1345–1347.
[8] J.Q. Sun, W.P. Chen, W. Xiang, W.C. You, Y. Zhuang, H.L.W. Chan, Degradation of $SrTiO_3$-based ceramic varistors induced by water and ac voltages, Ceramics International 33 (2007) 1137–1140.
[9] T.G. Wang, G.Q. Shao, W.J. Zhang, X.B. Li, X.H. Yu, Electrical properties of Pr_6O_{11}-doped WO_3 capacitor–varistor ceramics, Ceramics International 36 (2010) 1063–1067.
[10] V.V. Deshpande, M.M. Patil, V. Ravi, Low voltage varistors based on CeO_2, Ceramics International 32 (2006) 85–87.
[11] A.B. Glot, A.P. Zlobin, Nonohmic conductivity of tin dioxide ceramics, Inorganic Materials 25 (1989) 274–276.
[12] Z.M. Jarzebski, J.P. Marton, Physical properties of SnO_2 materials I, preparation and defect structure, Journal of the Electrochemical Society 123 (1976) 199C–205C.
[13] M. Batzill, U. Diebold, The surface and materials science of tin oxide, Progress in Surface Science 79 (2005) 47–154.
[14] D.D. Trung, N.V. Toan, P.V. Tong, N.V. Duy, N.D. Hoa, N.V. Hieu, Synthesis of single-crystal SnO_2 nanowires for NO_x gas sensors, Ceramics International 38 (2012) 6557–6563.
[15] H. Kim, H. Park, A study on the electrical properties of fluorine doped direct-patternable SnO_2 thin films, Ceramics International 38 (2012) S609–S612.
[16] S.A. Pianaro, P.R. Bueno, E. Longo, J.A. Varela, A new SnO_2-based varistor system, Journal of materials science letters 14 (1995) 692–694.
[17] D.S. Melo, M.R.C. Santos, I.M.G. Santos, L.E.B. Soledade, M.I.B. Bernardi, E. Longo, A.G. Souza, Thermal and structural investigation of SnO_2/Sb_2O_3 obtained by the polymeric precursor method, Journal of Thermal Analysis and Calorimetry 87 (2007) 697–701.
[18] N. Dolet, J.M. Heintz, M. Onillon, J.P. Bonnet, Densification of $0.99SnO_2$–0.01CuO mixture: Evidence for liquid phase sintering, Journal of the European Ceramic Society 9 (1992) 19–25.
[19] J.A. Cerri, E.R. Leite, D. Gouvêa, E. Longo, J.A. Varela, Effect of cobalt (II) oxide and manganese (IV) oxide on sintering of tin (IV) oxide, Journal of the American Ceramic Society 79 (1996) 7999–8004.
[20] T. Kimura, S. Inada, T. Yamaguchi, Microstructure development in SnO_2 with and without additives, Journal of Materials Science 24 (1989) 220–226.
[21] S.J. Park, K. Hirota, H. Yamamura, Densification of non-additive SnO_2 by hot isostatic pressing, Ceramics International 11 (1985) 158.
[22] M.S. Castro, C.M. Aldao, Characterization of SnO_2-varistors with different additives, Journal of the European Ceramic Society 18 (1998) 2233–2239.
[23] H.K. Lin, H.C. Chiu, H.C. Tsaia, S.H. Chien, C.B. Wang, Synthesis, characterization and catalytic oxidation of carbon monoxide over cobalt oxide, Catalysis Letters 88 (2003) 169–174.
[24] C.B. Wang, H.K. Lin, C.W. Tan, Thermal characterization and microstructure change of cobalt oxides, Catalysis Letters 94 (2004) 69–74.
[25] J.A. Aguilar-Martínez, M.I. Pech-Canul, M. Esneider, A. Toxqui, S. Shaji, Synthesis, structure parameter and reaction pathway for spinel-type Co_2SnO_4, Materials Letters 78 (2012) 28–31.
[26] S.A. Pianaro, E.C. Perreira, L.O.S. Bulhoes, E. Longo, J.A. Varela, Effect of Cr_2O_3 on the electrical properties of multicomponent ZnO varistors at the pre-breakdown region, Journal of Materials Science 30 (1995) 133–141.
[27] G. Brankovic, Z. Brankovic, M.R. Davolos, M. Cilense, J.A. Varela, Influence of the common varistor dopants (CoO, Cr_2O_3 and Nb_2O_5) on the structural properties of SnO_2 ceramics, Materials Characterization 52 (2004) 243–251.
[28] W.K. Bacelar, P.R. Bueno, E.R. Leite, E. Longo, J.A. Varela, How Cr_2O_3 influences the microstructure and no nohmic features of the SnO_2 (Cox, Mn_{1-x})O-based varistor system, Journal of the European Ceramic Society 26 (2006) 1221–1229.